

Toward a Unified AGN Structure

DEMOSTHENES KAZANAS^{1,2}, KEIGO FUKUMURA^{2,3}, EHUD BEHAR⁴,
 IOANNIS CONTOPOULOS⁵
 AND
 CHRIS SHRADER^{2,6}

ABSTRACT

We present a unified model for the structure and appearance of accretion powered sources across their entire luminosity range from galactic X-ray binaries to luminous quasars, with emphasis on AGN and their phenomenology. Central to this model is the notion of MHD winds launched from the accretion disks that power these objects. These winds provide the matter that manifests as blueshifted absorption features in the UV and X-ray spectra of a large fraction of these sources; furthermore, their density distribution in the poloidal plane determines the “appearance” (i.e. the column and velocity structure of these absorption features) as a function of the observer inclination angle. This work focuses on just the broadest characteristics of these objects; nonetheless, it provides scaling laws that allow one to reproduce within this model the properties of objects spanning a very wide luminosity range and viewed at different inclination angles, and trace them to a common underlying dynamical structure. Its general conclusion is that the AGN phenomenology can be accounted for in terms of three parameters: The wind mass flux in units of the Eddington value, \dot{m} , the observer’s inclination angle θ and the logarithmic slope between the O/UV and X-ray fluxes α_{OX} . However, because of a significant correlation between α_{OX} and UV luminosity, we conclude that the AGN structure depends on only two parameters. Interestingly, the correlations implied by this model appear to extend to and consistent with the characteristics of galactic X-ray sources, suggesting the presence of a truly unified underlying structure for accretion powered sources.

¹Email: Demos.Kazanas@nasa.gov

²Astrophysics Science Division, NASA/Goddard Space Flight Center, Greenbelt, MD 20771

³University of Maryland, Baltimore County (UMBC/CRESST), Baltimore, MD 21250

⁴Research Center for Astronomy, Academy of Athens, Athens 11527, Greece

⁵Department of Physics, Technion, Haifa 32000, Israel

⁶Universities Space Research Association

Subject headings: accretion, accretion disks — galaxies: active — methods: numerical — quasars: absorption lines — X-rays: galaxies

1. Introduction

The notion of AGN as an astronomical object of solar system dimensions and luminosity surpassing that of a galaxy has been with us for about half a century now. Since then, the advent of novel observational techniques, the accumulation of data and theoretical modeling has refined and advanced our notions as to what constitutes an AGN, with accretion onto a black hole as the source of the observed radiation now being universally accepted. At the same time, the discovery of galactic bright X-ray binary (XRB) sources, powered also by accretion onto compact objects (neutron stars and stellar size black holes) has extended the notion of accretion powered source to the stellar domain. Indeed, the general similarity of the X-ray spectral properties of AGN and galactic black hole candidates (GBHC) and XRBs in general, including their broad Fe $K\alpha$ fluorescence features (Miller 2007), argues for near horizon structures which are very similar, despite the huge disparity in the objects' scales. This structure is thought to consist of a Shakura-Sunyaev (Shakura & Sunyaev 1973) disk that extends to the ISCO (innermost stable circular orbit) of the corresponding flow, supplemented by an overlying hot, X-ray emitting corona.

Even though it is generally accepted that the AGN radiant energy is released by the accretion of matter onto a black hole (or in certain cases by extraction of the hole's rotational energy) in a region comparable to its horizon, there is plenty of evidence that a significant fraction of the AGN power is emitted, after reprocessing, at much larger radii. [One should note however, that accretion energy can also be transported outward not only radiatively but also mechanically by the viscous stresses that transport the accretion flow's angular momentum (Blandford & Begelman 1999)]. Thus, the UV and optical lines that constitute, typically, a fraction $f \sim 10\%$ of the AGN bolometric luminosity, are emitted presumably by clouds at distances $\sim 0.1 - 10$ pc that cover a fraction f of the AGN solid angle. In addition to the line emission, the AGN ionizing continuum is also reprocessed into IR and far-IR radiation by matter at even larger distances, which apparently subtends an even larger fraction of the AGN solid angle ($\sim 50\%$). The geometry of this component is thought to be cylindrical (rather than spherical) with a column density that depends strongly on the angle θ of the observers' line of sight (LoS) with the symmetry axis. It was proposed that such a geometry nicely unifies the Seyfert-1 and Seyfert-2 AGN subclasses (Antonucci & Miller 1985) and also those of the broad and narrow line radio galaxies (BLRG - NLRG) (Barthel 1989), according to the angle θ : Thus, Seyfert-1s (or BLRG) are AGN in which the observer's LoS makes a small angle with their axis of symmetry, the column of the intervening cold

gas is small ($N_H < 10^{21}\text{cm}^{-2}$) and the continuum source and its surrounding broad line emission (concentrated in the inner AGN regions) are directly visible. Seyfert-2s (or NLRG) on the other hand, represent the same objects viewed at a large inclination angle, along which the column density to the source is much larger ($N_H > 10^{23}\text{cm}^{-2}$), obscuring the continuum source and allowing the view of only the large distance (hence narrow component) of the emission lines. This obscuring structure is referred to as the “AGN molecular torus”, considering that it must consist of gas in molecular state, given its low effective temperature ($T \sim 10 - 100$ K). Statistics of Seyfert-1 and Seyfert-2 AGN imply that the height h of these torii must be comparable to their distance R from the AGN center, i.e. $h/R \simeq 1$. However, the value of this ratio is in conflict with that implied by hydrostatic equilibrium and the ratio of their thermal ($v_{\text{th}} \sim 1 (T/100\text{K})$ km/s) and Keplerian ($v_K \sim 300 - 500$ km/s) velocities, namely $h/R \simeq v_{\text{th}}/v_K \sim 10^{-3}$, thus presenting us with a conundrum concerning the physics of these structures.

These spectroscopically inferred components, along with observations of narrow radio jets along the AGN symmetry axis, led to the now well known AGN picture of (Urry & Padovani 1995), which consists simply of their arrangement at the appropriate positions in the AGN vicinity. Compelling as this picture might be observationally, it includes very little, if any, of the underlying physics. The AGN constituent components are independent of each other with physical properties assigned as needed by the observations of the specific objects. However, more recent observational developments suggest that such a picture is rather incomplete. To begin with, Boroson & Green (1992) have shown the existence of interrelations among AGN the line properties and also relations to other bands of the spectrum (notably the X-rays). Then, the increase in UV spectral resolution afforded by *HST* has shown that roughly 50% of Seyfert-1s exhibit UV absorption troughs due to plasma outflowing at $v \simeq 300 - 1000$ km/s, too narrow to have been discerned by the earlier *IUE* observations (Crenshaw et al. 1999), which did detect some, but in a much smaller fraction of the overall AGN population. To these flows one must also include those of the so-called BAL QSOs, which reach velocities along the observer’s LoS in excess of 10^4 km/s (Weymann et al. 1991). These are observed in about $\simeq 10\%$ of high luminosity quasars, implying that they subtend a similar fraction of the continuum source solid angle in these objects.

In addition to these UV absorption features, outflowing components were also found in the AGN X-ray spectra. The increase in spectral resolution provided by *ASCA* showed that approximately 50% of Seyfert-1s exhibit also blue-shifted absorption features in their X-ray spectra (George et al. 2000), indicative of outflowing plasma, but of different ionization state than that responsible for the UV absorption features. More recently, Tombesi et al. (2010a) have shown that Fe-K absorption features at velocities $v \sim 0.1c$ are rather common in nearby Seyfert galaxies and coined for them the term ultra-fast outflows (UFO). The simultaneous presence of both UV and X-ray absorbers in the same objects implies they belong to the same outflowing plasma (see e.g. Gabel et al. 2003). However, despite a large

number of studies supporting this hypothesis, (Mathur et al. 1994; Mathur, Elvis & Wilkes 1995; Collinge et al. 2001; Crenshaw et al. 2003; Brandt et al. 2009), an understanding of the underlying gas dynamics is lacking. A common origin for the plasma of these components as features of a common, radiatively driven flow would be hard to reconcile with their different velocities and ionization properties.

An account of the observed AGN outflows, in particular of the most challenging high velocity ones of BAL QSOs was put forward semi-analytically by Murray et al. (1995). These authors, in analogy with the winds of O-stars, proposed that they are driven off the inner regions of the QSO accretion disks by UV and optical line radiation pressure to achieve velocities consistent with those observed. The same issue was taken up in more detail in 2D numerical calculations by Proga, Stone, & Kallman (2000) who included in these calculations the detailed photoionization of the line driven wind by the QSO X-ray radiation. As shown in this work, efficient wind driving by line pressure requires that the line driven wind material be shielded from the ionizing effects of the X-rays, otherwise line driving becomes ineffective. Their calculations showed that the “failed wind” from the highly ionized innermost regions of the AGN accretion disk did provide the required shielding. The fact that BAL QSOs are weak X-ray emitters appears to advocate for such a point of view.

The ubiquity of AGN outflows implies that they should be included in the AGN structure schematic of Urry & Padovani (1995); however, the broad range of observed velocities and their different values in the UV and X-ray bands make such a construct complicated in the absence of an underlying unifying principle. However, such attempts have been made. Thus, Elvis (2000), motivated by the velocity fields produced by Proga, Stone, & Kallman (2000) in modeling the BAL QSO outflows, proposed a scheme that would supplement the AGN picture of Urry & Padovani (1995) with outflow components consistent with observed phenomenology. By limiting the fast ($v \gtrsim 10^4$ km/s), radiatively driven flow to a narrow angular sliver ($\Delta\theta \simeq 6^\circ$) around $\theta_s \simeq 50^\circ$ (Proga, Stone, & Kallman 2000), he accounted for the observed fraction of BAL QSOs in the overall QSO population. He then attributed the lower velocities of the typical X-ray and UV absorption features to the projection effects of viewing this flow at a larger angle ($\theta > \theta_s$) and the absence of absorption features in fraction of the objects to the low column and high ionization of the wind at $\theta < \theta_s$. He also postulated that the angular position θ_s and the opening angle $\Delta\theta$ of the high velocity radiatively driven radial stream would vary with source luminosity in a way that could account the variation of source properties with luminosity. However, his approach ignored the outflows seen in the AGN X-ray spectra, which at the time were not as well documented.

The AGN picture proposed herein is in the same spirit as that of Elvis (2000) in that, employing a well defined wind dynamical model, it provides a framework of systematizing the multitude of observational facts, in particular the more recent high resolution X-ray spectroscopy observations. However, it does more than that; it provides, in addition, scaling arguments similar to those put forward by Boroson (2002), which allow one to incorporate

within this single framework the ionization properties of Seyferts, BAL QSOs and XRBs, the structure of the AGN molecular torii and the corresponding IR spectra. This is possible because the underlying dynamical models, which span many decades in radius, are to a large extent independent of the mass of the accreting object and, as such, they can be applied to objects over a very wide range of luminosity. As we will discuss in the ensuing sections, the models we present provide the possibility of a broader classification of the structure of accreting sources in terms of a small number of parameters (2) thus providing an opportunity for a unified treatment of all accretion powered sources. The present work will concentrate on the structure of AGN, however it will be argued that the structures of XRBs are quite similar, their appearance being different only because of their very different ionization.

In §2 we provide a brief review of AGN outflow phenomenology with emphasis on the more recent high spectral resolution observations of X-ray absorbers by *Chandra* and *XMM-Newton*. In §3 we present our model and its general scalings. In §4 the model is applied to produce the absorber properties of galactic and extragalactic objects as specific cases of its parameters along with its general structure properties, depicted in two diagrams that relate the absorber column, velocity and observation angle. In §5 we focus on the emission properties of these winds and provide an account of the observed linear relation between the $H\alpha$ and bolometric AGN luminosities as well as their IR-to-far-IR spectra. Finally in §6 the results are reviewed and directions for future research are outlined.

2. X-Ray Spectroscopy and Warm Absorbers

Following the discovery of the ubiquitous nature of X-ray absorption features (Warm Absorbers) in the *ASCA* spectra, the launch of *Chandra* and *XMM-Newton* ushered a new era in the study of these features. Their superior sensitivity and resolution compared with those of previous missions made clear the presence of a plethora of transitions (see e.g. Behar et al. 2003) in the spectra of numerous AGN. For example, the X-ray bright QSO IRAS 13349+2438 ($z = 0.10764$) and the Seyfert-1 galaxy (e.g. MCG-6-30-15 at $z = 0.007749$) observed extensively with *ROSAT* (Brandt, Fabian & Pounds 1996) and *ASCA* (Brandt et al. 1997) gave indications of absorption features in the sub-keV regime. Their *Chandra* and *XMM-Newton* spectra confirmed this fact and exhibited a wealth of transitions such as N VII, Ne VII–Ne X, Mg V–Mg XII, Na XI, Si VI–Si XIV, and Ni XIX while successfully identifying almost all charge states of Fe and O in some cases (Behar et al. 2003; Holczer et al. 2007, hereafter HBK07). Furthermore, these observations showed the various transitions to be blueshifted relative to the host galaxy, indicating that the warm absorber plasma is, in fact, outflowing.

Though the majority of the X-ray absorber features in the *Chandra* and *XMM-Newton* archives are associated with the spectra of Seyfert galaxies, absorption features have been

also seen in the spectra of quasars; these are mainly Fe-K features usually at velocities higher than those seen in Seyferts, in the range of $v/c \sim 0.1-0.8$, suggesting launching of these winds from regions very close to the compact object. These include both BAL [see Chartas et al. (2003) for PG 1115+080, Chartas et al. (2007) for H 1413+117, Chartas et al. (2002, 2009) for APM 08279+5255; as such these also exhibit high velocity UV absorption features] as well as non-BAL quasars [see Pounds et al. (2003) for PG 0844+349, Reeves et al. (2003) for PDS 456, Pounds & Page (2006) for PG 1211+143]. The columns of these features are $N_H \sim 10^{23} - 10^{24} \text{ cm}^{-2}$ which are typically at least ~ 10 times higher than that of UV absorbers (Srianand & Petitjean 2000; Chartas et al. 2009). Finally, as discussed above, Fe-K features at velocities $v > 10^4 \text{ km/s}$, have been detected in a large fraction ($\sim 1/3$) of observed AGN. Tombesi et al. (2010a) refer to these as ultra-fast outflows (UFO).

Absorption features of varying ionization states have also been observed in galactic sources (GBHC, XRB) (e.g. Miller et al. 2008; Neilsen, Remillard & Lee 2011; Brandt & Schulz 2000). Considering that the presence of the ionic species observed in these sources, like in AGN, is due to photoionization of an outflow by the photons of the continuum source, their distribution is determined by the photoionization parameter $\xi = L/nr^2$, where L is the ionizing luminosity, n the local gas density and r the distance of this gas from the source. The higher S/N ratios of galactic sources afforded better determination of the velocities of the different ions as well as the densities of the outflowing wind at a given radius r . Based on these parameters, it was concluded (see e.g. §3.1) that the wind of GRO 1655-40 (Miller et al. 2008) cannot be driven by the radiation pressure or by the X-ray heating of this source and therefore it must be driven by the action of magnetic fields (e.g. Blandford & Payne 1982; Contopoulos & Lovelace 1994). Similar analysis of the X-ray spectra of GRS 1915+105 by Neilsen, Remillard & Lee (2011) concluded that the wind mass flux at the outer edge of its accretion disk (associated with the lowest ionization ions) could be as much as twenty times larger than the mass flux needed to power the source’s X-ray luminosity, while a similar conclusion was reached by Behar et al. (2003) concerning the wind of NGC 3783. Finally, it should be noted here that the wind velocities of the highest ionization species (Fe-K) are significantly smaller in GBHC than in Seyferts, which in turn are smaller than those of BAL QSOs, a fact that should be accounted within the general framework of any wind model.

2.1. The Absorption Measure Distribution

The very detection in the AGN X-ray spectra of species of such diverse states of ionization as Fe XXV, Mg V and O I is an important fact in itself. It implies a wind with density distribution that produces ionic columns, sufficiently large to be detected, for ions that “live” at widely different values of ξ and, most likely, also at widely different distances from the ionizing source. This alone is a significant constraint on outflow models. Taking this argument

into consideration, Holczer et al. (2007) and subsequently Behar (2009) fit the ensemble of the absorber data in the X-ray spectra of a number of AGN with a continuous distribution in ξ (rather than adding components of different ξ until a sufficiently low χ^2 is achieved). In doing so, they developed a statistical measure of the plethora of the transitions in the *Chandra/XMM-Newton* X-ray spectra, the absorption measure distribution (AMD). This is the hydrogen equivalent column density of specific ions, N_H , per decade of ionization parameter ξ , as a function of ξ , i.e. $AMD(\xi) = dN_H/d\log \xi$. For a monotonic distribution of the wind density $n(r)$ with the radius r , determination of AMD is tantamount to determining the ionized wind’s density dependence on r (along the observers’ LoS). Therefore, considering that $AMD \propto N_H$, a power law dependence on ξ of the form $AMD \propto N_H \propto \xi^\alpha$, implies also a power law dependence for the wind density on r i.e. $n(r) \propto r^{-s}$ with $s = (2\alpha + 1)/(\alpha + 1)$. So for $\alpha \simeq 0$ (AMD independent of ξ), $s \simeq 1$, consistent with the conclusion reached by Behar (2009).

As noted in Behar (2009), an $n(r) \propto 1/r$ density profile is inconsistent with the asymptotic dependence of a mass conserving spherical wind which obtains $n(r) \propto r^{-2}$ and whose ionization parameter “freezes” to a constant value ξ_∞ . On the other hand, considering that the velocity of such winds is achieved only asymptotically, with the velocity having the general behavior $v(r) = v_\infty(1 - r_*/r)$ (Murray et al. 1995), the AMD would exhibit in this case too a dependence on ξ at radii $r \lesssim r_*$. Assuming a mass conserving spherical wind with the above velocity structure, i.e. $n(r)v(r)r^2 = \dot{m} = const.$, one can easily deduce that

$$\frac{dN_H}{d\log \xi} \sim N_H(\xi) = \frac{\dot{m}}{v_\infty r_*} \left[\frac{\xi_\infty}{\xi} - 1 \right] \quad (1)$$

where ξ_∞ is the ionization parameter at infinity. Under the above velocity field, near r_* , the wind base, ξ (and also v) approaches zero and the gas column diverges so that $AMD \propto N_H \simeq (\dot{m}/v_\infty r_*)(\xi_\infty/\xi)$. At large distances, with $\xi = \xi_\infty - \epsilon$, ($\epsilon/\xi_\infty \ll 1$), $N_H = (\dot{m}/v_\infty r_*) \epsilon$, so that the absorption measure distribution has the form $AMD \propto (\epsilon/\xi_\infty) \propto r_*/r$, i.e. the wind column decreases like r^{-1} , as expected. The arguments leading to the above scalings are certainly overly simple, however they show that for radiatively driven winds, the column *decreases* with *increasing* ionization and *increasing* velocity, in significant disagreement with the dependence found by Holczer et al. (2007) and Behar (2009); they also suggest that in attempting to account for the AMD behavior, one should search for wind models with density and velocity profiles asymptotically different from those driven by radiation pressure.

While it is hard to produce radiation pressure driven winds with the density profile implied by the AMD, i.e. $n(r) \propto r^{-1}$ (even an extended source of radiation asymptotically appears point-like and the winds acquire density $n(r) \propto r^{-2}$), MHD winds off accretion disks were known to provide such density profiles for some time now (Contopoulos & Lovelace 1994, hereafter, CL94). These are generalizations of the two dimensional MHD winds enunciated by Blandford & Payne (1982) in that they allow also for mass flux rates which depends on the radius. Given that the velocities of these winds asymptotically scale like

the disk Keplerian velocity at the point of launching, i.e. $v \propto r^{-1/2}$, one can then easily see that for $n(r) \propto r^{-1}$, $\dot{m}(r) \propto r^2 n(r) v(r) \propto r^{1/2}$, i.e. the wind mass flux \dot{m} increases with distance. In this respect these winds follow the ADIOS prescription discussed by Blandford & Begelman (1999). The specific density profile inferred from the AMD is interesting in that it provides equal column per decade of radius. As such, it is consistent with the density needed to account for the lags in the power spectra of XRB and AGN (Kazanas et al. 1997; Papadakis et al. 2001) in terms of Compton scattering. Finally, this same profile for the dust density of AGN winds, at radii beyond the dust sublimation radius, was employed by Königl & Kartje (1994) and Rowan-Robinson (1995) to produce Seyfert-2 and QSO IR-spectra in agreement with observations. The fact that this wind density profile can accommodate in a natural way several diverse and independent aspects of AGN phenomenology under the same framework is suggestive of its central role in the AGN structure and appearance.

3. The Model MHD Winds

Motivated by the straightforward interpretation of the AMD in terms of density profiles associated with MHD winds, we outline in this section some properties of these wind models with emphasis on their scalings with the black hole mass, mass flux rate and distance. We pay particular attention on the scalings of the winds' ionization and columns, as these are related to the observations of X-ray absorbers.

The MHD winds considered here are launched by accretion disks threaded by poloidal magnetic fields under the combined action of rotation, gravity and magnetic stresses as discussed in Blandford & Payne (1982). To simplify the treatment it is assumed that the wind is axisymmetric and as such one need only solve the field geometry and fluid flow in the poloidal (r, θ) -plane. To simplify further the problem one looks for solutions separable in r and θ with power law r -dependence for all magnetic field and fluid variables. After consideration of all conserved quantities in the poloidal plane (mass flux per magnetic field flux, angular momentum, magnetic line angular velocity and Bernoulli integral) one is left with the force balance in the θ -direction (the so-called Grad-Safranov equation). The solution of this equation provides the angular dependence of all the fluid and magnetic field variables with their initial values given on the surface of the disk at $(r_o, 90^\circ)$, where r_o is a fiducial radius that sets the radial scale of the system and it is of order of the Schwarzschild radius, r_S . The Grad-Safranov equation has the form of a wind equation with several critical points, the most important of which for our purposes the Alfvén point; this can be crossed by appropriately choosing the flow boundary conditions on the disk surface (see CL94, BP82).

The scalings of the magnetic field, velocity, pressure and density are given by

$$\mathbf{B}(r, \theta) \equiv (r/r_o)^{-(s+1)/2} \tilde{\mathbf{B}}(\theta) B_o, \quad (2)$$

$$\mathbf{v}(r, \theta) \equiv (r/r_o)^{-1/2} \tilde{\mathbf{v}}(\theta) v_o, \quad (3)$$

$$p(r, \theta) \equiv (r/r_o)^{-(s+1)} \mathcal{P}(\theta) B_o^2, \quad (4)$$

$$n(r, \theta) \equiv (r/r_o)^{-s} \tilde{n}(\theta) B_o^2 v_o^{-2}. \quad (5)$$

The density normalization is given in terms of the poloidal field on the disk B_o , however, it is more instructive to express it in terms of the accretion or wind outflow rate \dot{m} as discussed in FKCB10; then the density normalization at the inner edge of the disk at $\theta = 90^\circ$ is given on setting $\tilde{n}(90^\circ) = 1$ by

$$n_o = \frac{f_W \dot{m}_o}{2\sigma_T r_S}, \quad (6)$$

where f_W is the ratio of the mass-outflow rate in the wind to the mass-accretion rate \dot{m}_o , assumed here to be $f_W \simeq 1$, and σ_T is the Thomson cross-section. It is important to note here that because the mass flux in these winds depends in general on the radius, the normalized parameter used throughout this work, \dot{m}_o , always refers to the mass flux at the innermost value of the flow radius, i.e. at $r/r_o \equiv x \simeq 1$. With the scalings given above we then have $\dot{m}(x) = \dot{m}_o x^{-s+3/2}$, so for $s = 1$, as inferred from the fits of HBK07, $\dot{m} \propto x^{1/2}$ (the Blandford & Payne (1982) solution has $s = 3/2$, so $n(r) \propto x^{-3/2}$ and therefore $\dot{m} \propto x^0$ or $d\dot{m}/d\log x = \text{const.}$).

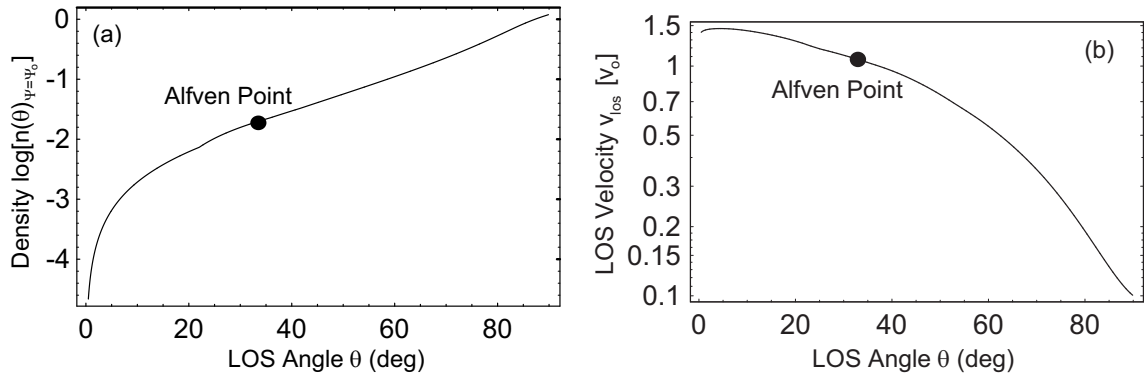


Fig. 1.— (a) Wind density as a function of the polar angle θ normalized to its value on the disk surface ($\theta = 90^\circ$). (b) The line of sight wind velocity on a given field line, normalized to the Keplerian velocity of the foot point of the specific field line v_o .

3.1. Scaling Laws

The reason that the winds we present here can be applied to AGN as well as to GBHC, as mentioned above, is that winds and flows in general are known to be self-similar when: The radius r is normalized to the Schwarzschild radius r_S ($x = r/r_S$, $r_S = 3M$ km, where

$M = M/M_\odot$ is the mass of the accreting object M in units of the solar mass M_\odot); the mass flux \dot{M} is expressed in units of the Eddington accretion rate $\dot{M}_E = L_E/c^2$ (L_E is the Eddington luminosity, $L_E \simeq 1.3 \cdot 10^{38} M \text{ erg s}^{-1}$) as $\dot{m} = \dot{M}/\dot{M}_E \propto \dot{M}/M$; their velocities are Keplerian, i.e. $v \simeq x^{-1/2} c$.

While the wind scalings of eqs. (2) - (5) were introduced for the solution of the MHD equations one can write quite general scaling laws that incorporate those of the above equations as special cases. We do so now both for accretion flows and winds and use them to produce scalings for expressions of the wind density, column density, ionization parameter and AMD as a function of the dimensionless radius x , the dimensionless mass flux rate \dot{m} and black hole mass M .

1. Accretion: In applying the scalings of eqs. (2) - (5) to spherical accretion one obtains for the density $n(x) \propto x^{-3/2} \dot{m} M^{-1}$ and for the column density $N_H(x) \propto x^{-1/2} \dot{m}$, i.e. an expression *independent* of M ; so, flows onto objects of widely different masses but of the same $\dot{m} = \dot{M}/\dot{M}_E$ have the same column at the same distance x from the accreting object; its normalization is such to yield Thomson depth $\tau_T \simeq 1$ for $x \simeq 1$ at $\dot{m} \simeq 1$ (this is the similarity of Advection Dominated Accretion Flows (ADAF) of (Narayan & Yi 1994)).

2. Winds: Analogous considerations of similarity apply equally well to winds, given that, generally, their asymptotic velocity, v_∞ , is proportional to the Keplerian velocity at the wind launching radius, r_l , i.e. $v_\infty \propto x_l^{-1/2}$, with $x_l = r_l/r_S$. So mass conservation in physical and dimensionless units reads respectively

$$\dot{M} \sim n R^2 v_\infty \quad \text{and} \quad \dot{m}_W M \propto n(x) x^2 M^2 x_l^{-1/2} \quad (7)$$

with \dot{m}_W denoting in this case the mass outflow rate in units of the Eddington rate \dot{M}_E . Therefore, the wind density and local column density are given in dimensionless units correspondingly by the expressions (dropping the subscript W from \dot{m}_W)

$$n(x) \propto \frac{\dot{m} x_l^{1/2}}{M x^2} \quad \text{and} \quad N_H(x) \propto \dot{m} \frac{x_l^{1/2}}{x} \quad (8)$$

with the object mass M again dropping out of the expression for the column density N_H . For 1D winds, e.g. stellar winds or winds driven by the intense radiation pressure near a compact object, x_l is roughly constant and $N_H(x) \propto \dot{m}/x$, i.e. the wind column decreases inversely proportionally to the distance. However, in the more general case of 2D winds (e.g. those of BP82 and CL94) where the wind is launched from a wide range of radii in an accretion disk with, generally, different mass flux rates at each radius, $x_l \sim x$, $\dot{m} = \dot{m}(x)$ and $N_H(x) \propto \dot{m}(x) x^{-1/2}$ and numerically $N_H(x) \simeq 10^{24} \dot{m}(x) x^{-1/2} \text{ cm}^{-2}$ (it should be understood that $n(x)$, $N_H(x)$ have an additional angular dependence discussed in the previous section). As noted in Blandford & Begelman (1999) winds with position dependent \dot{m} are the means by which 2D accretion flows dispose of the excess energy and angular momentum transferred

mechanically by the viscous stresses from the smaller to the larger radii, so that finally only a small fraction of the available mass accretes on the compact object (BB99). For wind density of the form $n(x) \propto x^{-s}$, the mass flow rate varies with x like (BB99)

$$\dot{m}_W(x) = \dot{m}_o x^{-s+3/2}, \quad s \leq 3/2, \quad (9)$$

with \dot{m}_o being the mass outflow from the smallest radius $x \sim 1.5 - 3$; for $s = 1$, $\dot{m} \propto r^{1/2}$ and N_H constant per decade of r .

3. Photoionization: The wind ionization is determined by the local ratio of photons to electrons, the ionization parameter $\xi = L/n(r)r^2$, (L is the source's ionizing luminosity – different from the total luminosity, $n(r)$ the local density and r the distance from the ionizing source). This can also be expressed in dimensionless units: If η ($\simeq 10\%$) is the radiative efficiency of the accretion process, then the luminosity L can be written as $L \propto \eta \dot{m}_a M$ (\dot{m}_a is the accretion rate that reaches the compact object to produce the luminosity L), or $L \propto \eta \dot{m}_a^2 M$ in the case of ADAF (Narayan & Yi 1994) [i.e for $\dot{m}_a \lesssim \alpha^2$ with α the disk viscosity parameter], yielding the for ξ an expression also independent of M , implying similarity in wind ionization, whether in AGN or XRB (FKCB10)

$$\xi(x) \simeq \frac{L}{n(r)r^2} \simeq \begin{cases} \frac{\eta \dot{m}_a}{N_H(x)x} \simeq 10^8 \frac{\eta}{f_W} \frac{1}{x^{-s+2}} & \text{for } \dot{m}_a > \alpha^2 \text{ (non-ADAF)} \\ \frac{\eta \dot{m}_a^2}{N_H(x)x} \simeq 10^8 \frac{\eta}{f_W} \frac{\dot{m}_a}{x^{-s+2}} & \text{for } \dot{m}_a < \alpha^2 \text{ (ADAF)} \end{cases} \quad (10)$$

where $f_W = \dot{m}_o/\dot{m}_a$ (~ 1) is the ratio of mass flux in wind and accretion at the smallest radii and s the index of the density dependence on r . These relations are also independent of M , implying a similarity in the ionization structure of winds, whether in AGN of any type or GBHC. For a spherical wind, ($s = 2$) the ionization parameter is independent of x (asymptotically), while for $s = 1$ it decreases linearly with distance from the ionizing source.

4. The AMD: Writing Eq. (10) as $N_H(x) \propto \eta \dot{m}_a / \xi(x)x$ one can form the expression for AMD (HBK07), namely

$$AMD = \frac{dN_H(x)}{d \log \xi(x)} \simeq \frac{\eta \dot{m}_a}{\xi(x)x} \quad (11)$$

The fact that AMD is largely independent of $\xi(x)$ (HBK07) implies $\xi(x) \propto 1/x$ or $N_H(x) \propto \log(x)$, $n(x) \propto 1/x$ and $\dot{m} \propto x^{1/2}$, i.e. the wind mass flux increases with radius, as discussed in BB99. In this case, both the ionization parameter and the wind density decrease like $1/r$ while the column of the ions found at a given ξ remains roughly constant, in broad agreement with Behar (2009). So, in disks of sufficiently large radial extent, the wind launched at their larger radii will be of sufficiently low ionization and temperature to conform with the properties of the AGN unification torus. Finally, one should bear in mind that the above scaling laws do not include the θ –dependence of the density and the column density (see fig. 1). At a given (radial) distance r from the source, this leads to much higher ionization

of the plasma flowing along the symmetry axis and even smaller neutral absorption column than along the higher column density, less ionized equatorial directions, in agreement with the unification considerations (Königl & Kartje 1994).

Under the above scaling laws, the ionization, velocity and AMD of the winds discussed in this work are independent of the mass of the accreting object. Therefore these expressions should hold equally well for AGN and GBHC or XRB in general, a fact in obvious disagreement with observation, given their very different X-ray absorber properties. This would indeed be the case if the ionizing spectrum were also independent of the mass of the accreting object. However, *the similarity of wind ionization is finally broken by the dependence of the ionizing (X-ray) flux on the mass of the accreting object and leads to the different wind ionization properties not only between XRB and AGN, but also amongst AGN*: Both in AGN and XRB a major fraction of their bolometric luminosity is emitted in quasithermal features referred to as the Big Blue Bump (BBB) in AGN and the Multi Color Disk (MCD) in XRB. Both are thought to represent emission of the accretion luminosity in black body form by a geometrically thin optically thick disk of size a few Schwarzschild radii. The characteristic temperature of this feature scales as $M^{-1/4}$, being in the X-ray band for solar mass objects and in the UV for AGN of $M \sim 10^8 M_\odot$. This dominance of the ionizing luminosity (X-rays) as a fraction of the bolometric one in XRB over AGN is, according to our model, the main cause for their differences in their wind ionization properties as it will be discussed in detail in the next section. Even within AGN, the ionizing flux is in fact not a constant fraction of the bolometric luminosity but it depends on the absolute source luminosity. A measure of their ionizing luminosity is given by the index α_{OX} , the logarithmic slope of the flux between 2500 Å and 2 keV. This quantity has a strong dependence on $L(2500 \text{ Å})$ (Steffen et al. 2006; Brandt et al. 2009), a fact that bears relation to the corresponding AGN absorber properties, as it will be discussed in the next section.

4. The Ionization Structure of MHD Winds

With the wind structure set by the solution of the Grad-Safranov equation, one can now proceed to study its ionization structure. The details are given in Fukumura et al. (2010a) so we simply restrict ourselves to a broad description of this procedure. Given the (approximately) $1/r$ density profile, we have split the radius along a given LoS from r_o to $10^6 - 10^8 r_o$ in approximately 40 segments, spaced equally in $\log r$, so that each has the same column density. Then we assume a value for \dot{m}_o which provides the normalization of the wind density through Eq. (6) (we generally assume $f_W = 1$) and a luminosity L related to \dot{m}_o either as $L = 1.3 \cdot 10^{38} \dot{m}_o M \text{ erg/s}$ or $L = 1.3 \cdot 10^{38} \dot{m}_o^2 M \text{ erg/s}$ (for $\dot{m}_o < \alpha^2$, according to the ADAF prescription) with a specific spectrum; then we invoke the photoionization code XSTAR to compute the ionization, opacity and emissivity of the first zone. Using the derived

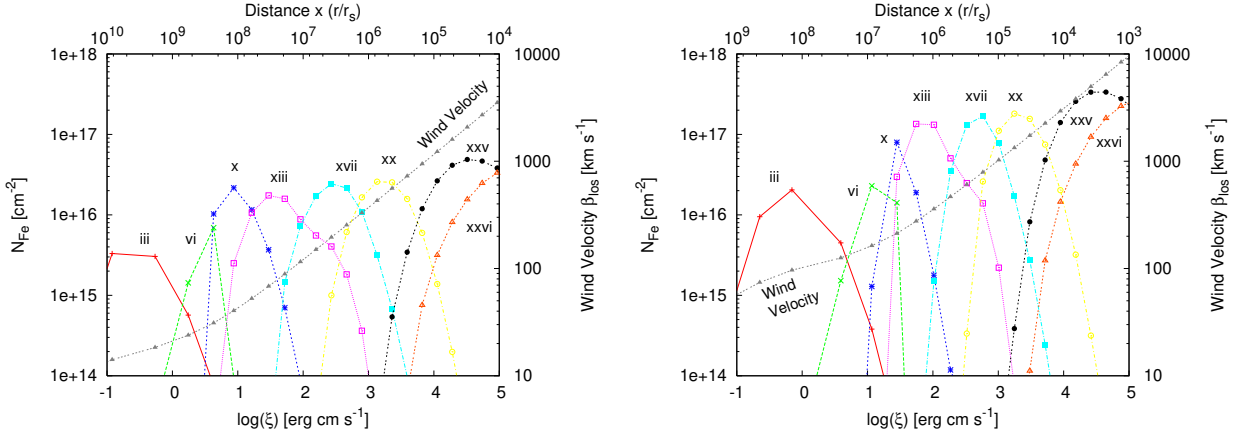


Fig. 2.— The ionization structure of iron appropriate for a Seyfert galaxy with $\dot{m}_o \simeq 0.1$ and an ionizing photon spectrum with $dF_\nu/d\nu \propto \nu^{-\Gamma}$, $\Gamma = 1.9$, as seen at two different inclination angles $\theta = 30^\circ$ (left) and $\theta = 60^\circ$ (right). The ionization decreases with increasing distance r along a given LoS and with increasing θ for a given value of r . The column of each ion is given in the left ordinate, while the velocity at each position along the LoS in the right one. The LoS velocity at each ξ (lower abscissa) and the corresponding radius (upper abscissa) is given by the black triangles.

opacities and emissivity we compute the spectrum exiting this zone, which is used as the input for computing the ionization opacity and emissivity of the next zone. The procedure is repeated to compute the ionization of the wind along a given line of sight and then for different values of the polar angle θ , to produce the ionization structure of the wind over the entire poloidal plane.

Fig. 3 of Fukumura et al. (2010a) depicts the density and ionization structure of such winds out to $10^8 r_o$ in linear coordinates. One can see that the wind ionization depends both on the distance from the source r and on the angle θ , being highly ionized at small values ($\xi \gtrsim 10^3$ near $\theta = 0$) even at these large distances, while it decreases to $\xi < 1$ at $\theta \sim 80^\circ$. It is also clear that for a given θ , a harder X-ray spectrum will ionize the wind out to larger distances. Since the wind velocity along a given LoS depends mainly on the radius of launching the specific parcel of gas (but also the inclination angle θ), absorption features associated with a given ion should appear at smaller velocities the harder the ionizing spectra. This issue is in fact a little more complicated because we only observe the wind velocity along our line of sight which depends also on the local shape of the poloidal magnetic field lines.

4.1. Ionization of XRB Winds

The high X-ray content of the spectra of XRB, implies that they should be, in general, much more ionized than those of AGN. Nonetheless, X-ray absorption features have also been observed in XRBs, as indeed seems to be the case. So P-Cygni Fe-K features were first detected in Cir X-1, which is (presumably) an accreting neutron star in a 16.6 day binary orbit around a main sequence companion (Brandt & Schulz 2000; Schulz & Brandt 2002). The high ionization of the inner sections of these outflows, render them essentially devoid of any absorption features. Therefore, the highest ionization species Fe XXVI, Fe XXV should occur at radii such that $\xi \lesssim 10^4$, which, as the authors suggest sets them at distances $r \simeq 10^5$ km and corresponding velocities of only $v \simeq 1,000$ km/s.

There are several other XRB in which similar features have been detected, the best known being GRO 1655-40 (Miller et al. 2006, 2008) and GRS 1915+105 (Neilsen, Remillard & Lee 2011) both of which show Fe XXVI and Fe XXV absorption features at velocities similar to those of Cir X-1. GRO 1655-40 presents a multitude of absorption features similar to those of AGN, however, because of the higher S/N ratio their velocities and EW are better determined and thus more constraining to the outflow models. Following detailed modeling it was concluded (Miller et al. 2006, 2008) that the wind of GRO 1655-40 is not consistent with being driven by either line radiation pressure or thermally by the X-ray heating of the outer regions of the disk. The authors then concluded that the only reasonable means of driving the outflow in this object is magnetic, via an MHD wind similar to those outlined in this work.

GRS 1915+105 affords a similar analysis (Neilsen, Remillard & Lee 2011, and references therein). Detailed photoionization modeling of this source provided both the column and velocity associated with specific transitions. Assuming that the line absorbing medium has thickness $\Delta r \simeq r$, and that the observed velocities are effectively Keplerian, i.e. $v/c \simeq (r/r_S)^{-1/2}$, one can obtain simultaneous estimates of both r and v ; these along with the measured absorption column $N_H \simeq nr$ yield an estimate of the mass flux of the wind, which it was found that it could be as much as several times larger than the mass accretion rate needed to power the observed X-ray emission of this source. In fact, one is led to a similar conclusion concerning the mass flux in the wind of Cir X-1 by using the parameters provided in Schulz & Brandt (2002), indicating that a wind mass flux increasing with r may not be an uncommon feature in accretion powered sources.

Finally, it is worth noting that the disks of all three of the above sources are apparently at high inclinations, i.e. directions that favor observations of such features (less ionization, higher column densities). For lower inclination systems, the winds are likely far more highly ionized, yielding no apparent absorption features.

4.2. Ionization Structure of Seyfert Winds

The procedure outlined in §4 describing the detailed calculation of the ionization of MHD winds was applied to winds associated with Seyfert galaxies (Fukumura et al. 2010a). As noted above, given the scale invariance of the wind column and ionization parameter, the main difference between the ionization winds off the disks of different classes of accretion powered sources (e.g. XRB, Seyferts, BAL QSOs) is the spectrum of the ionizing radiation. Since for Seyfert galaxies the X-ray and UV-optical luminosities are approximately the same, we have approximated the ionizing spectra with a single power law from 1 – 1,000 Rydberg of photon index $\Gamma = 1.9$ and for the accretion rate we used the value of $\dot{m}_o = 0.1$.

The 2D density and poloidal plane ionization structure of a wind for the above parameters is given in Fig. 3 of Fukumura et al. (2010a). Here, we present in Figure 2 the ionic species distribution of just one element of this wind, namely iron, as a function of the distance from the continuum source (upper abscissa) and the corresponding value of ξ (lower abscissa), for two different values of the observer inclination angle $\theta = 30^\circ, 60^\circ$ (left and right panels respectively). The column of each ionic species is given in the left ordinate, while the corresponding velocity along the LoS is given in the right ordinate and represented by the black triangles.

We can see that increasing θ increases the column of a specific ionic species. Also, because the radius at which it now forms is smaller, the velocity at the peak abundance of this ion is correspondingly higher. Finally, one can obtain the AMD of this flow by adding the columns of all ions of Fe at a given value of ξ . As expected, and shown explicitly in (Fukumura et al. 2010a), this is constant (i.e. independent of the value of ξ or the value of r/r_S), reflecting the column per decade of radius of the underlying wind.

The ionization properties of Seyfert galaxies are consistent with the models presented in this figure. The conclusions of Behar (2009), based on the AMDs of the five AGN he has analyzed are broadly consistent with ours as presented in this section. Some of them require slightly steeper density profiles ($s \simeq 1.25$) whose ionization structure and velocity properties should be similar to those presented in this section.

4.3. Ionization Structure of BAL QSO Winds

If the tenets of the proposed model are correct, it should be able to reproduce the velocity and ionization structure of the absorption features of accretion powered objects other than Seyfert galaxies through judicious choices of the values of the available parameters. Should such an enterprise be successful, it could delineate the regions of parameter space occupied by individual AGN classes and hence provide their systematization on the basis of an underlying physical model.

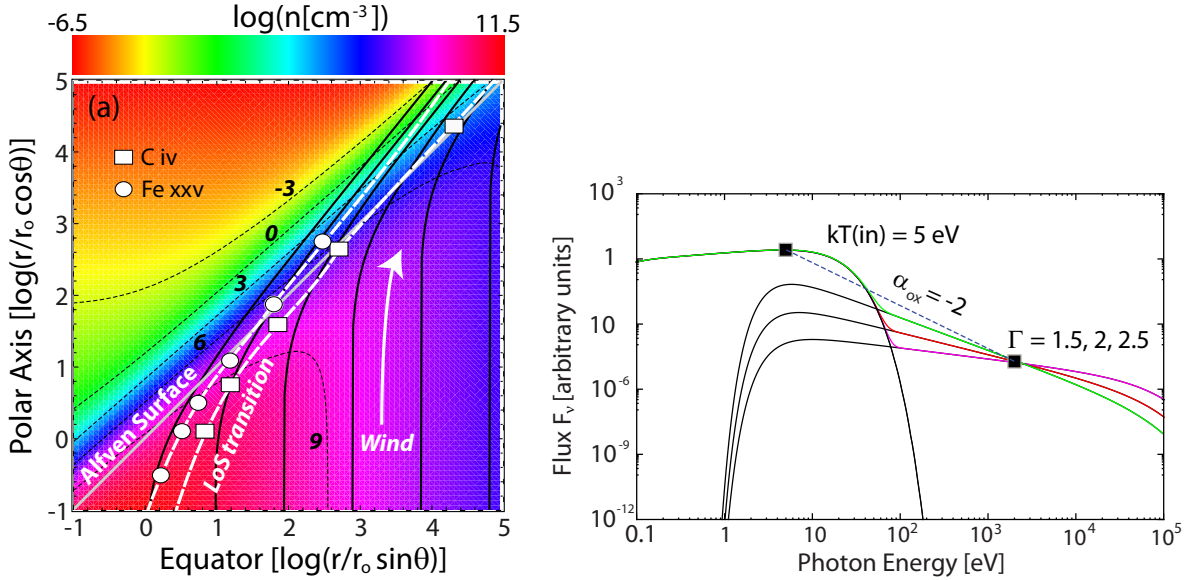


Fig. 3.— (a) 2D poloidal plane density structure of an MHD wind of $\dot{m} = 0.1$ and $M = 10^9 M_\odot$, ionized by the spectrum shown in (b). The density, $\log(n[\text{cm}^{-3}])$, is shown in color with the dotted lines being the iso-density contours, with the log of the corresponding density indicated by the associated numbers. The r, z coordinates are in logarithmic scale, so lines of increasing θ are lines at 45° inclination of increasing abscissa intercepts. Also shown are the magnetic field lines (*black solid*) and the loci (*white dashed lines*) of the positions of formation of Fe XXV (circles) and C IV (squares). (b) The form of the SED used to produce the wind ionization of (a) consisting of (i) a thermal MCD (as BBB) spectrum of innermost temperature $kT_{\text{in}} = 5$ eV and (ii) a power-law continuum of photon index Γ . The X-ray flux is normalized relative to that of BBB by α_{ox} . [See the electronic edition of the *Journal* for a color version of this figure.]

Such an attempt was made by Fukumura et al. (2010b), who employed the specific MHD winds to model the absorption features in the spectra of BAL QSOs, in particular that of APM 08279+0255 (Chartas et al. 2002, 2003). This AGN class was chosen because the properties of absorption features of its members are most different from those of Seyferts, since they exhibit Fe XXV at velocities $v \simeq 0.5c$ and C IV at $v \simeq 0.1c$. Because these objects were selected on the basis of their broad UV absorption features, any such model should be able to provide an account of the *combined* properties of both their X-ray and UV features.

The property that most clearly separates Seyferts and BAL QSOs is the relative weakness of their X-ray to their UV luminosity. This is reflected in the corresponding value of their α_{OX} parameter, which in BAL QSOs has values $\alpha_{\text{OX}} \simeq -2$ compared to -1 to -1.2 for Seyferts. To model the ionization of BAL QSO winds, Fukumura et al. (2010b) have chosen as ionizing spectrum that shown in Fig. 3b. This consists of a BBB component of maxi-

imum temperature 5 eV along with a power law component of photon index Γ , normalized at $E = 2$ keV relative to the BBB so that it results in $\alpha_{OX} = -2$, consistent with that of APM 08279+0255. The decrease in the value of α_{OX} is significant, because it implies that the ratio of ionizing photon density (given by the X-rays) to the matter density (represented by the luminosity of the BBB that peaks in the UV) is quite small, yielding a value for the ionization parameter at $r \simeq r_o$ much smaller than that of Seyfert galaxies. Furthermore, the cooling effects of the prominent UV emission further contributes to lowering the gas temperature at the smallest radii and hence its ionization. It is then possible that some of the heavy elements (e.g. Fe) will not be fully ionized even at wind radii $r \simeq r_o$, leading to a high outflow velocity for Fe XXV, Fe XXVI.

The presence of non-fully ionized Fe at radii $r \gtrsim r_o$, along with the very steep (unobservable) EUV source spectrum, depletes severely the photons at energies $E \gtrsim 50$ eV needed to produce the ion C^{+3} of carbon. Since this ion forms at a specific value of ξ , this suppression of ionizing photons is made up by a decrease in the radius r at which it forms (and an increase in the local wind velocity), leading to CIV absorption features at velocities much higher than those of Seyfert galaxies. Figure 3a shows in logarithmic scale the density distribution of a wind of $\dot{m}_o = 0.1$, and $M = 10^9 M_\odot$. Dashed lines are the isodensity contours with the logarithm of the corresponding density denoted by the assigned number, while the thick black lines are the lines of the poloidal magnetic field. The wind flow in the poloidal plane is along the magnetic field lines, while the observers' LoS (radial coordinates) correspond to lines of 45 degree inclination; an increasing inclination angle θ corresponds to increasing abscissa intercepts for these lines. The white circles and squares along with their connecting curves indicate correspondingly the positions of formation of the Fe XXV and CIV transitions for observers at different values of θ . The ionization structure of the wind can thus be translated into the spatial localization of specific ionic species. With a judicious choice of θ ($\simeq 50^\circ$) one can obtain $r(\text{Fe XXV}) \sim 5 - 40 r_S$ and $r(\text{CIV}) \sim 300 - 900 r_S$ (assuming a single LoS) to produce absorption velocities for these transitions consistent those of the BAL QSO APM 08279+0255.

In Fig. 4 we show the hydrogen equivalent columns of several ions of iron and carbon as a function of the ionization parameter ξ for a LoS at an angle $\theta = 50^\circ$ and for the ionizing spectrum given in Fig. 3b. This is a figure equivalent to those for Seyferts shown in Fig. 2 but appropriate for a BAL QSO. The figure shows also the corresponding wind velocity along this LoS (red dashed line), while the shaded regions indicate the positions of maximum column for Fe XXV and CIV, which are indicative of the observed velocity of the corresponding ion.

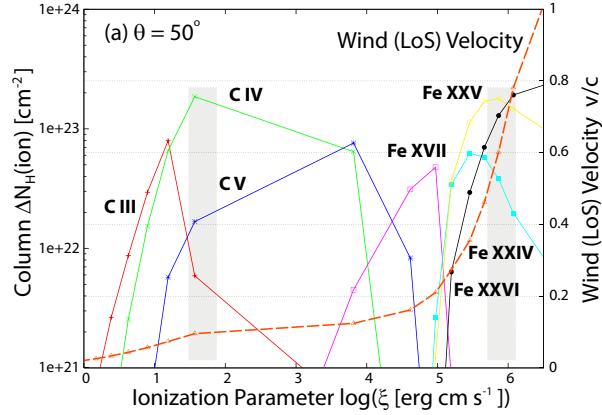


Fig. 4.— Simulated distribution of local column densities ΔN_H (on the left ordinate) and the outflow LoS velocity v/c (on the right ordinate) as a function of ionization parameter ξ for (a) C and (b) Fe with $\theta = 50^\circ$. Vertical lines denote the ionization parameter where the local emergent column is dominated primarily by C IV in (a) and Fe XXV in (b), respectively, also showing the corresponding outflow velocity v/c . [See the electronic edition of the Journal for a color version of this figure.]

4.4. The Characteristic Curves of Ionized MHD Winds

The previous two subsections have shown that, while the underlying velocity structure of MHD winds may be very similar and their overall column depending only on the dimensionless mass flux \dot{m}_o , their ionization structure and the location of specific ions in these winds can be quite different depending on their ionizing spectra. Under these (admittedly oversimplified) assumptions one can present the kinematic properties of specific ionic species of these winds into two diagrams that encapsulate their essential features (namely velocity and column) as a function of the ionizing radiation spectral properties and the observers' LoS.

Such diagrams for the transitions C IV($\lambda\lambda 1548, 1551\text{\AA}$) and Fe XXV are shown in Figs. 5a,b. The C IV characteristic curves are shown in blue while those of Fe XXV in red. In Fig. 5a, appropriate for an observer at $\theta = 50^\circ$, we show: (i) The correlations between the C IV, Fe XXV velocities and the X-ray photon index Γ for $\alpha_{OX} = -2$ (solid lines, left ordinate). (ii) The correlation between the C IV, Fe XXV velocities and the source α_{OX} for an X-ray photon slope $\Gamma = 2$ (dashed lines, right ordinate). The pairs in parentheses indicate the values of (Γ, α_{OX}) at each point.

We observe that the velocities of both C IV and Fe XXV depend more strongly on α_{OX} than on Γ . However, for $\alpha_{OX} = -2$, as is the case with APM 08279+0255, the Fe XXV velocity changes significantly with Γ and in a way that is actually in agreement with the observations

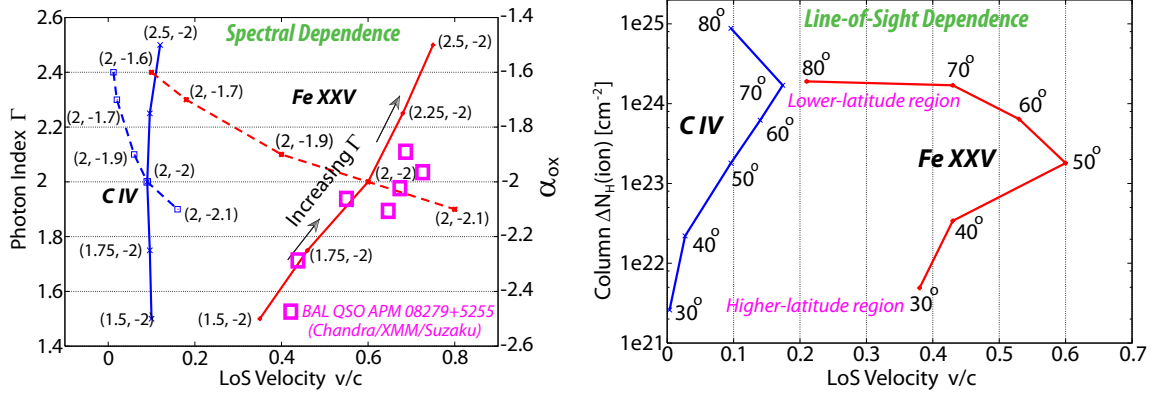


Fig. 5.— (a) The dependence of the model wind LoS velocity (for $\theta = 50^\circ$) on Γ (solid lines; left ordinate) and α_{OX} (dashed lines; right ordinate). The ordered pairs at each point are the values of (Γ, α_{OX}) for C IV (blue lines) and Fe XXV (red lines). The red squares indicate the change in the Fe-K absorption velocity variations with Γ for APM 08259+5255. (b) The model MHD wind correlation between the LoS velocity of a given transition (blue for C IV, red for Fe XXV) and the corresponding hydrogen equivalent column $\Delta N_H(\text{ion})$ with the observer inclination angle θ as a parameter along these curves (indicated by the numbers in degrees). [See the electronic edition of the Journal for a color version of this figure.]

of Chartas et al. (2009), given by the squares along the solid red curve. The C IV velocity appears to be much less sensitive to Γ , however it is quite sensitive to the value of α_{OX} , ranging between $v \simeq 0.15c$ and $0.01c$ as α_{OX} varies from -2.1 to -1.6 , nicely covering the observed range of the velocity of this transition between BAL QSO and Seyferts.

In Fig. 5b we show the correlation between the LoS velocity of the specific ions (i.e. C IV, FeXXV) for a wind ionized by a source with $\alpha_{OX} = 2$, $\Gamma = 2$ (values appropriate for a BAL QSO), and the corresponding hydrogen equivalent columns, N_H , with the LoS inclination angle as a parameter along these curves. For these specific spectral parameters, we see that both velocities increase with θ up to a critical value different for each transition and then level-off as the corresponding ions are produced in parts of the wind that it is still accelerating. It is also worth noting that even for the specific spectral distribution, appropriate for BAL QSOs, the velocity of C IV is quite small for sufficiently small observer inclination angle, while at the same time the corresponding column may be too small for the detection of such a feature. Diagrams such as that of Fig. 5b for different ionizing spectra and wind parameters will be useful for the determination of the wind parameter space (N_H, v) at which specific features become observable. We expect to provide several such diagrams for the most important such transitions in future works.

5. Wind Emission Properties

The models and computational setup outlined in the previous were motivated by and dealt mainly with the absorption feature properties of accretion powered sources, both galactic and extragalactic. However, besides the absorber properties, the reprocessing of radiation onto these winds provides also emission characteristics, both in continuum and in lines. These will be given a first brief treatment in this section, which serves mainly as the road map of future work. So in section 5.1 we discuss the effects of dust reprocessing into continuum while in 5.2 reprocessing into lines and specifically that of $H\alpha$.

5.1. Torus Structure and Infrared Emission

The issue of AGN torii and their importance in unification schemes was discussed in the introduction. Also outlined there was the conundrum of the disparity between their (statistically inferred) height-to-radius ratios ($h/R \simeq 1$) and the values implied by the ratio of their thermal to Keplerian velocities ($h/R \simeq v_{\text{th}}/v_{\text{K}} \simeq 10^{-3}$). The proposal that resolves this conundrum in a straightforward fashion is that of Königl & Kartje (1994) who suggested that the torii are not structures in hydrostatic equilibrium, but dynamical objects, in particular MHD winds driven-off the outer environs of the AGN disks. Furthermore, in fitting the observed IR emission as disk UV radiation reprocessed in these winds, they concluded that the corresponding density of the reprocessing gas had to be proportional to $1/r$ as in the winds discussed in §3.

Similarly, Rowan-Robinson (1995) has shown that reprocessing the AGN continuum luminosity by dust can provide good fits to their (nearly flat in νF_ν) IR spectra, provided that the dust density has a profile similar to that used herein, namely proportional to $1/r$. There is no mystery here: Dust distribution with the specific density profile reprocesses the same amount of continuum flux per decade of radius and re-emits it in (roughly) black body form; since the dust temperature in regions of increasing radius r falls-off like $T \propto r^{-1/2}$ the peak emission will also shift to lower frequencies while emitting the same luminosity; the resulting spectrum would then be “flat” in νF_ν units, consistent with the *Spitzer* observations of a survey of QSO spectra (Netzer et al. 2007).

The precise spectrum determination depends, of course, on the details of dust formation and properties and also on the details of the reprocessed spectrum and radiative transfer, as the emission is not necessarily black body and as the outer layers of the MHD wind reprocess not only the continuum luminosity but also the IR emission of the inner “torus” regions. One of the more important aspects of the IR and far-IR emission is the frequency at which the spectrum turns over from “flat” to the Rayleigh-Jeans form ($\nu F_\nu \propto \nu^3$), as this would provide an estimate of the outer torus radius. Combined space (*Herschel*) and ground

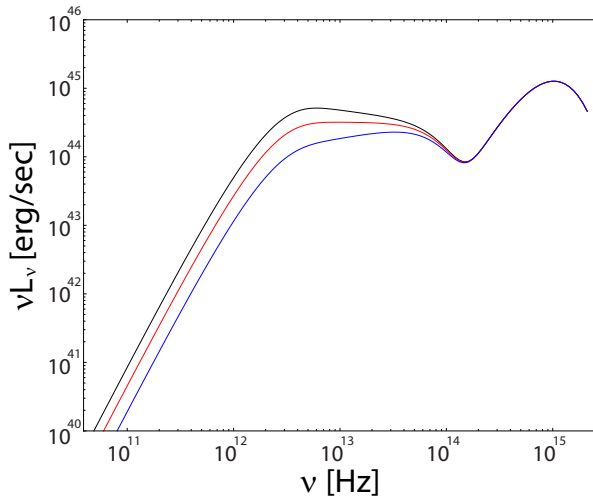


Fig. 6.— Model spectra resulting from reprocessing the BBB AGN continuum (with peak at $\nu \simeq 10^{15}$ Hz) by winds with three different density profiles $s = 0.9$ (black), $s = 1.0$ (red), $s = 1.1$ (blue), that extend roughly two orders of magnitude beyond the dust sublimation radius. [See the electronic edition of the Journal for a color version of this figure.]

(ALMA) observations will be instrumental in this respect. One should simply note here that the radial dust temperature dependence, $T \propto r^{-1/2}$, implies that the number of decades in radius over which dust reprocessing takes place is twice the number of decades over which the AGN νF_ν spectrum is “flat”. In this respect, there should be a synergy between AGN X-ray spectroscopy and far-IR observations: The regions at which the far-IR emission turns over to the Rayleigh-Jeans form (the “edge” of the torus) are comparable to those at which the lowest ξ ions should be located; the “edge” of the torus should then manifest then also in the X-ray spectra as a steep drop in the X-ray column with decreasing ξ . Finally, one should note that IR spectra similar to those of Seyfert-2 galaxies are not expected in XRB, despite their similarity of their winds; this is because the distance at which the dust sublimation temperature ($T \sim 1000$ K) is reached in the wind of an XRB of $L = 10^{37}$ erg s $^{-1}$, is larger than 10^{12} cm, the typical XRB binary separation distance.

Fig. 6 presents an oversimplified example of such a spectrum. In there we present the reprocessing of the BBB spectrum of an AGN (the component that peaks near $\nu \sim 10^{15}$ Hz), by dust which extends from the radius of dust sublimation to the “edge” of the torus, a region that spans roughly two decades in radius. The dust density in this region has a form $n(r) \propto r^{-s}$ with $s = 0.9, 1, 1.1$ (black, red and blue curves respectively) to indicate the effect that different density profiles on the far-IR AGN spectra. In this specific case the AGN is viewed “face-on” and the reprocessing is effectively limited to $\theta \gtrsim 50^\circ$. The details of the X-ray obscuration and its relation to IR emission, bearing relation to the angular

distribution of our solutions, can be improved with combined X-ray – IR surveys such as that of (Rowan-Robinson et al. 2009).

5.2. H α Emission of MHD Winds

The issue of line emission in AGN is a subject far too broad to be included in any detail in the present work. Nonetheless, to our surprise, we found that the basic model we have been discussing so far is consistent with well known features and correlations concerning the *emission line* properties of AGN and XRB. So we do make a brief foray into this subject to touch upon two issues on which our model seems to provide a novel insight.

One of the fundamental characteristics of the winds outlined in section 3 are that their velocity fields are mainly Keplerian at low latitudes ($\theta \gtrsim 70^\circ$) while becoming (almost) radial at larger ones (Contopoulos & Lovelace 1994; Fukumura et al. 2010a). This particular property allows for the possibility of exhibiting emission line features associated both with disks and winds. In fact, there are observations of a “double horn” H α line profile in certain AGN (Eracleous & Halpern 1994), the tell-tale sign of disk emission. These have been modeled as emission excited by the reprocessing of the AGN X-ray continuum on a ring-like structure, whose radii and illumination were adjusted to provide agreement with observations. The MHD wind models in their most simplistic incarnation, namely that described §3, allow for such profiles for the H α transition, precisely because of the disk-like geometry of the flow at low latitudes. Furthermore, the extent of the wind in the θ –direction allows also the *calculation* of the EW of this transition, which is found to be consistent with observations (Fukumura & Kazanas in preparation).

The calculations outlined in §4 provide the photonionization of the entire wind, from its smallest ($x \gtrsim 1$) to its largest ($x \sim 10^5 - 10^7$) scales, set by the size of the accretion disk that powers the source. With the wind ionization given, one can also produce scalings and correlations involving properties of the corresponding emission of lines of the photoionized plasma. While such an in-depth study is beyond the scope of the present paper, some straightforward scalings can be produced even at this early stage. With this in mind, we compute below the scaling of one of the prominent transitions AGN, namely H α with the source luminosity, given that such a relation has already been well documented (Osterbrok 1989) (we refrain focusing on the Ly α and C IV transitions since, being resonant ones, demand a more careful treatment within the specific model).

Quite generally, the luminosity of the H α transition produced in the MHD winds discussed in the previous sections can be written as

$$L_{\text{H}\alpha} \simeq \alpha(T) n^2 V \epsilon_{\text{H}\alpha} \quad (12)$$

where $\alpha(T)$ is the recombination coefficient, $n^2 V$ the wind emission measure and $\epsilon_{\text{H}\alpha} \simeq 2$

eV, is the H α energy. As noted in Eq. (5), the wind density is given by the expression $n(r, \theta) \simeq n_o \tilde{n}(\theta) x^{-1} \dot{m}/M$, where $\tilde{n}(\theta) \simeq e^{(\theta-\pi/2)/0.22}$. The normalization n_o is set so that $n_o r_o \sigma_T \simeq 1$ for $\dot{m} \simeq 1$ in spherical geometry. For the same value of the total mass flux, since the flow in the MHD winds considered herein is concentrated near the equatorial plane, the density normalization must be higher by a factor $A \simeq 1/\int_0^{\pi/2} \tilde{n}(\theta) \sin\theta d\theta \simeq 1/0.21$ with the density profile now reading $n(r, \theta) \simeq n_o A \tilde{n}(\theta) x^{-1} \dot{m}/M$. Then the emission measure of the wind reads

$$n^2 V = 2\pi n_o^2 \frac{\dot{m}_o^2}{M^2} r_o^3 M^3 x_m 2 \int_0^{\pi/2} A^2 \tilde{n}(\theta)^2 \sin\theta d\theta \quad (13)$$

$$\simeq 10\pi n_o^2 r_o^2 \sigma_T^2 \frac{r_o}{\sigma_T^2} x_m \dot{m}_o^2 M \simeq 7.1 \times 10^{49} r_o \dot{m}^2 M x_m \quad (14)$$

where the extra factor of 2 in front of the integral takes care of the emission by both hemispheres, the numerical value of the integral is $\simeq 2.5$, σ_T is the Thomson cross section and we have taken for the (normalized in units of r_S) maximum radius of the disk the value $x_m \sim 10^6$, with $r_o \simeq r_S \simeq 3 \times 10^5$ cm, the Schwarzschild radius of one solar mass. Then, the H α line luminosity will be

$$L_{H\alpha} \simeq \alpha(T) n^2 V \epsilon_{H\alpha} \simeq 2 \cdot 10^{36} \dot{m}_o^2 M \text{ erg s}^{-1} . \quad (15)$$

At the same time, the accretion luminosity will be

$$L \simeq 10^{38} \eta \dot{m}_o M \quad (16)$$

where $\eta \simeq 0.1$ is the accretion disk radiative efficiency ($\eta \simeq 0.3$ for neutron stars and $L \propto \dot{m}_o^2 M$ in the case of ADAF).

The obvious point to note between Eqs (15) and (16) is that they both are proportional to the object's mass M ; also for $\dot{m}_o < \alpha^2$ (α is the accretion disk viscosity parameter) implying that the accretion flow is in the ADAF regime, the ratio $R = L_{H\alpha}/L$ of the line to the bolometric accretion luminosity is independent of both \dot{m}_o and the mass M . This ratio depends only on the recombination coefficient $\alpha(T)$ (with assumed value $\sim 10^{-13} \text{ cm}^3 \text{ s}^{-1}$ in Eq. (15) above) and the disk efficiency η and has a value $R \simeq 1/20 - 1/50$. The data indicating the correlation between the H α line and the continuum luminosity at $\lambda 4800 \text{ \AA}$ is shown in Fig. 7. The data shown are those of 11.6 of Osterbrok (1989) with the abscissa converted from flux to luminosity; this figure includes in addition the H α luminosity of Cir X-1 (filled square; Johnston et al. 1999), a galactic XRB; inclusion of this point in the figure is important because it almost doubles the dynamic range of this relation which now covers eight decades in the line luminosity $L_{H\alpha}$. The H α luminosity of this source falls slightly below the extrapolation of a linear relation from AGN to XRB. A likely reason for this could be the reduced emissivity at small values of x (small radii) due to the higher gas temperature there. Incidentally, for winds with the density profile of the Blandford & Payne

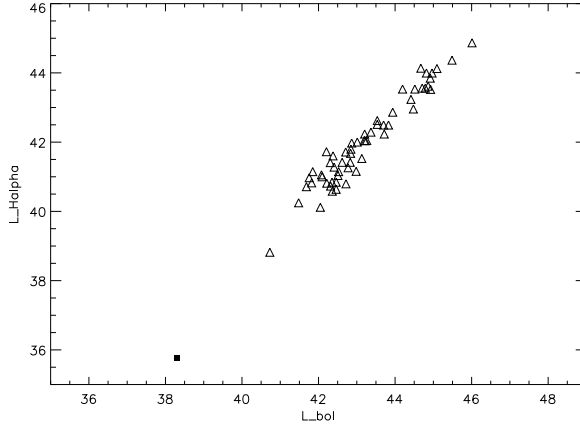


Fig. 7.— The H α luminosity of a number of AGN (triangles) as a function of their bolometric luminosity (taken to be their monochromatic luminosity at $\lambda = 4680 \text{ \AA}$, as given in Osterbrock 1989). The square denotes the H α luminosity of Cir X-1 given in Johnston et al. (1999) assuming the bolometric luminosity to be that of Eddington for a 1.4 solar mass neutron star.

(1982) scaling, i.e. $n(x) \propto x^{-3/2}$, Eq. (15) would be proportional to $\log x_m$ instead of x_m and the line luminosity would be roughly 10^5 times smaller than observed. We consider the straightforward, minimal assumption way that this model accounts for the linear relation between the H α and bolometric luminosities an indication of the validity of its fundamental premises.

6. Summary, Discussion

In the previous sections we presented a broad strokes picture of the 2D AGN structure, one that encompasses many decades in radius and frequency and supplements the well known schematic of Urry & Padovani (1995) with an outflow launched across the entire disk area and velocity roughly equal to the local Keplerian velocity at each launch radius. These outflows are responsible for the absorption features first detected in the AGN UV spectra and more recently established also in their X-ray ones. As noted in the introduction, the goal and the spirit of this paper is not to reproduce the detailed phenomenology of specific AGN spectral bands, but provide an account of their most general and robust trends; however, it purports to do so on the basis of a single, well founded, semi-analytic model for outflows off accretion disks that involves a small number of free parameters. In this same spirit, Fig. 8 presents a schematic of our model; the radius is in logarithmic space and the shading is indicative of the local *column* density in the spherical- r direction, which is constant, but has a strong dependence on the angle θ . The gray lines are illustrative of the magnetic field

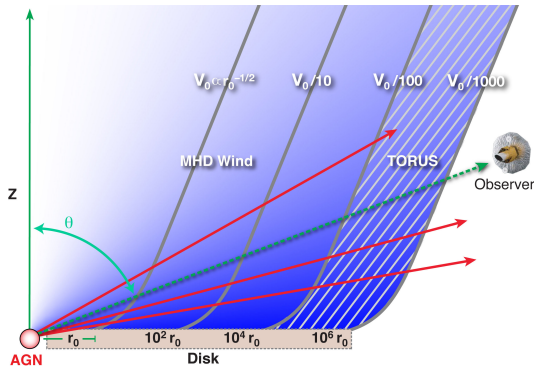


Fig. 8.— A schematic of the model presented in §3. The radius is shown in logarithmic scale, with the solid gray lines representing the poloidal field at each radius shown and the corresponding wind velocity relative to the fiducial one v_o . The shading is proportional to the local column in the r -direction which does not depend on r but has a strong θ -dependence as required by AGN unification. At sufficiently large distances, $r \gtrsim 10^4 r_o$ the flow is sufficiently cool to be molecular and acts as the torus required by AGN unification.

geometry with the corresponding scaling of the wind velocity on each one relative to the fiducial one v_o shown in the figure.

As shown in section §3, these outflows have the interesting property that their ionization and dynamical structures scale mainly with one parameter, the dimensionless accretion rate \dot{m} . As such, they are applicable, in principle, to all accretion powered sources from galactic accreting black holes to the most luminous quasars. The mass of the object, M , simply provides the overall scale of an object’s luminosity and size (and also a characteristic temperature for the BBB), in a way similar to that proposed by Boroson (2002).

However, despite this economy of parameters, because of the inherently 2D character of these winds, their appearance (and that of the AGN central regions) depends quite significantly on the observer’s inclination angle θ , a desirable feature and in agreement with our notions of AGN unification. Furthermore, and most importantly, as noted in section §4, the ionization structure of these flows depends also on the spectrum of the ionizing radiation. This dependence complicates the situation because it breaks the overall wind flow scale invariance on the mass M . As noted earlier, it is effectively the dependence of α_{OX} on luminosity which is responsible for the differences in the absorption feature properties between Seyferts and BAL QSOs. This dependence of α_{OX} on $L(2500\text{\AA})$ (and effectively on \dot{M}) suggests that eventually the wind ionization properties may constitute a two rather than three parameter family. Finally, the high ionization of the inner regions of these flows in XRB, naturally accounts for the low velocities of the Fe-K features observed in galactic sources.

The crucial and fundamental aspect of the underlying MHD wind model that allows the broad consolidation of the very diverse observational phenomenology of the previous sections “under the same roof” is their ability to produce density profiles that decreases like $\sim 1/r$ with the radius. It is this property that allows the ionization parameter to decrease with distance while still providing sufficient column to allow the detection of both high and low ionization ions in the AGN X-ray spectra. It is also this property that controls the velocities v of the Fe-K transitions in galactic sources, Seyferts and BAL QSO, due to the relation between v and ξ ($v^2 \propto \xi$ for the scaling proposed herein; the BP82 scaling leads to $v \propto \xi$ and therefore to much smaller velocity for a given ion, i.e. a given value of ξ – and also to a much smaller column). Furthermore, it is this specific density profile of the wind that allows us to incorporate the physics of the AGN torii within the context of the broader physics of accretion onto the compact object, while at the same time producing IR spectra in broad agreement with observation. This confluence of the AGN spectral properties with the wind spacial structure indicates that AGN and XRB are objects that span many decades in radius and frequency, despite the fact that most of their luminosity is released within a few Schwarzschild radii.

The price to pay for a density distribution such as that proposed above is the need to invoke winds whose mass flux increases with distance from the source (and more specifically like $\sim r^{1/2}$). While this feature can be accommodated by the choice of a parameter in the models of Contopoulos & Lovelace (1994), it was given a rather transparent explanation in Blandford & Begelman (1999), in terms of the dynamics of accretion. Interestingly, recent *Chandra* spectroscopy (Brandt & Schulz 2000; Behar et al. 2003; Neilsen, Remillard & Lee 2011) appear to support such a notion. At this point, it is not obvious how theoretically compelling is this particular feature in the general scheme of accretion properties. Why is this mass loss preferred to one that would result in, for instance, the BP82 density profile? Are there AGN with winds/accretion flows consistent with $n(r) \propto r^{-3/2}$? What parameter determines which one is chosen by nature? These are pressing questions for which we currently have no answers. However, the importance of the specific mass flux dependence on r in the interpretation of the AGN X-ray and UV absorber properties will likely attract the attention of future studies on this issue.

Clearly a presentation as broad as that above by necessity ignores a large number of issues, both observational and theoretical each of which is in fact a separate branch in the study of AGN physics. As such, we have ignored the effects of radiation pressure, considered in much detail numerically by Proga and collaborators (Proga, Stone, & Kallman 2000; Proga 2003; Proga & Kallman 2004) and semi-analytically by Murray et al. (1995). The effects of radiation pressure in combination with those of the MHD winds discussed here have been considered by Everett (2005) and also by Königl & Kartje (1994) in discussing the AGN IR spectra. These works have shown the effects of radiation pressure to be local, as they depend on the local flow opacity, thus breaking the similarity of the angular dependence

of the solutions. It was shown in these works that radiation pressure “pushes” to open up the field lines to produce a density dependence on θ different from that given in Fig. 2a and hence would influence the population ratios of objects observed at a given column density. However, the effects of radiation pressure do not affect the dependence of wind mass flux on the distance ($\dot{m} \propto r^{1/2}$), which is set by conditions on the disk; it is this property that determines the radial dependence of the wind density, the property necessary to account for their observed phenomenology.

As noted above, a radiation driven wind, while 2D in the region of launch, it will appear radial at sufficiently large distance producing density profiles $\simeq 1/r^2$ there. As appealing and compelling as the notion of radiation driven winds is, there is little evidence for them, at least in the AGN and XRB X-ray absorber spectra. Advocating radiation driven 2D winds across the entire accretion disk, in a fashion similar to those of §3, appears difficult because the photon field does not have enough momentum at these large distances to drive a wind with the required mass flux. Interestingly the ϕ –component of the magnetic field, decreasing like $B_\phi \propto 1/r$ has precisely the momentum needed to drive a wind with $\dot{m} \propto r^{1/2}$. In this respect one should bear in mind that these winds produce most of the kinetic energy at small radii, most of the mass flux at large radii and equal momentum per decade of radius.

Another issue that was only briefly touched upon in section 5, is that of line emission. It is generally thought that the line emission in AGN comes from clouds in pressure equilibrium with a hot intercloud medium, the result of the X-ray heating thermal instability (Krolik, McKee & Tarter 1981). Our simple estimates, even though they have ignored this possibility, they nonetheless provide an account for the observed correlation of the $H\alpha$ (a transition with minimal radiative transfer nuances) with the AGN bolometric luminosity. However, one should bear in mind that our model winds do allow for the formation of such clouds at sufficiently small latitudes (below the Alfvén surface) where the flow is close to hydrostatic equilibrium, i.e. under conditions of a given pressure. We expect that past the Alfvén point, where the flows are under conditions of given density, the formation of these clouds will be less forthcoming. The issue of cloud or wind AGN line emission is an issue that deserves more attention and study, given the smoothness of the AGN lines profiles that implies a very large number clouds involved in this process (Arav et al. 1997), but certainly beyond the scope of the present paper.

Our treatment of the AGN IR emission has also glossed over much of what it constitutes an altogether distinct subfield of AGN study. It has been suggested that clouds are also involved in this component of the AGN spectra, however with different properties and at radii larger than those of the UV and optical line emitting clouds (Nenkova et al. 2008). This is clearly a point that will have to be looked upon with greater care. A complicating factor in this direction is that of star formation in the AGN environment, whose IR contribution introduces additional parameters in such a study. Finally, with respect to the IR and far-IR AGN spectra, we would like to point to the synergy between X-ray spectroscopy and far-IR

observations discussed in §5.1 that would help establish the consistency of this scheme across two very different frequency bands.

Finally, we close with a few words on the “feedback” of our winds on the surrounding medium, which likely provides the mass that eventually “feeds” the AGN. First, the angular distribution of the flow, as determined by the poloidal field structure, due to its collimation, interacts with only part of the surrounding stellar cluster. Second, the energy flux of the winds considered here, despite their increasing mass flux with radius, is still dominated by the flux at small radii ($\dot{E} = \dot{m}v^2/2 \propto r^{-1/2}$); however, they do carry equal momentum per decade of radius ($\dot{P} = \dot{m}v \propto r^0$), a fact with potential feedback effects, perhaps the subject of a future publication. Finally, the radiation effects of the AGN are also limited in θ due precisely to the winds’ column increase with this parameter. However, as shown in Tueller et al. (2008), the fraction of *Swift-BAT* selected AGN at galactic latitude $|b| > 15^\circ$ with X-ray column $N_H > 10^{22} \text{ cm}^{-2}$ decreases from $\simeq 0.5$ to close to zero above luminosity $L \simeq 10^{44} \text{ erg s}^{-1}$. Therefore, considering that the observed column pertains not only to the AGN wind but also to the entire matter distribution along the LoS, the radiative effects of high luminosity AGN may affect significantly the evolution of their environment. Such constraints will have to be taken into account producing a global evolutionary sequence for our models, which are beyond the scope of the present paper.

Authors are grateful to Tim Kallman for insightful discussions and help with running *XSTAR*. K.F. and D.K. would also like to thank G. Chartas, J. Turner, L. Miller, S. Kraemer, T. Misawa for their constructive comments. D.K. would like to thank R. Mushotzky, C. Reynolds and C. Miller for discussions and the Astronomy Department of the University of Maryland for the hospitality during his sabbatical visit there.

REFERENCES

- Antonucci, R. R. J. & Miller, J. S. 1985, *ApJ*, 297, 621
- Arav, N., Barlow, T. A., Laor, A. & Blandford, R. D. 1997, *MNRAS*, 288, 1015
- Barthel, P. D. 1989, *ApJ* 336, 606
- Behar, E. et al. 2003, *ApJ*, 598, 232
- Behar, E., 2009, *ApJ*, 703, 1346
- Blustin, et al. 2005, *A&A*, 431, 111
- Boroson, T. A. & Green, R. F. 1992, *ApJS*, 80, 109

- Boroson, T. A. 2002, *ApJ*, 565, 78
- Brandt, W. N., Fabian, A. C., & Pounds, K. A. 1996, *MNRAS*, 278, 326
- Brandt, W. N., Mathur, S., Reynolds, C. S., & Elvis, M. 1997, *MNRAS*, 292, 407
- Brandt, W. N. & Schulz, N. S. 2000, *ApJ*, 544, L123
- Brandt, W. N., Laor, A., & Wills, B. J. 2000, *ApJ*, 528, 637
- Brandt, W. N., Chartas, G., Gallagher, S. C., Gibson, R. R., & Miller, B. P. 2009, arXiv:0909.0958v1
- Blandford, R. R & Begelman, M. C. 1999, *MNRAS*, 303, L1 (BB99)
- Blandford, R. D. & Payne, D. G. 1982, *MNRAS*, 199, 883 (BP82)
- Chartas, G., Brandt, W. N., Gallagher, S. C., & Garmire, G. P. 2002, *ApJ*, 579, 169
- Chartas, G., Brandt, W. N., Gallagher, S. C. 2003, *ApJ*, 595, 85
- Chartas, G., Eracleous, M., Dai, X., Agol, E., & Gallagher, S. C. 2007, *ApJ*, 661, 678
- Chartas, G., Saez, C., Brandt, W. N., Giustini, M., & Garmire, G. P. 2009, *ApJ*, 706, 644 (C09)
- Collinge, M. J. et al. 2001, *ApJ*, 557, 2
- Contopoulos, J., & Lovelace, R. V. E. 1994, *ApJ*, 429, 139 (CL94)
- Crenshaw, D. M. et al. 1999, *ApJ*, 516, 750
- Crenshaw, D. M. et al. 2003, *A.R.A.A.*, 41, 117
- Detmers, D. et al. 2011, *A&A*, 534, 38
- Elvis, M., et al. 1994, *ApJS*, 95, 1
- Elvis, M., et al. 1994, *ApJ*, 543, 686
- Eracleous, M. E. & Halpern, J. 1996, *ApJS*, 90, 1
- Everett, J. E. 2005, *ApJ*, 631, 689
- Fukumura, K., & Kazanas, D., Contopoulos, I., & Behar, E. 2010, *ApJ*, 715, 636 (FKCB10)
- Fukumura, K., & Kazanas, D., Contopoulos, I., & Behar, E. 2010, *ApJ*, 723, L228)

- Gabel, et al. 2003, ApJ, 583, 178
- Gallagher, S. C., Brandt, W. N., Sambruna, R. M., Mathur, S., & Yamasaki, N. 1999, ApJ, 519, 544
- Gallagher, S. C., Brandt, W. N., Chartas, G., Priddey, R., Garmire, G. P., & Sambruna, R. M. 2006, ApJ, 644, 709 (G06)
- George, I. M. et al. 2000, ApJ, 531, 52
- Green, P. J., & Mathur, S. 1996, ApJ, 462, 637
- Grevesse, N., Noels, A., & Sauval, A. 1996, in “Cosmic Abundances” ASP Conference Series, 99, S. Holt and G. Sonneborn, eds.
- Holczer, T., Behar, E. & Arav, N. 2010, ApJ, 708, 981
- Holczer, T., Behar, E., & Kaspi, S. 2007, ApJ, 663, 799
- Hewett, P. C., Foltz, C. B., & Chaffee, F. H. 1995, AJ, 109, 1498
- Hewett, P. C., & Foltz, C. B. 2003, AJ, 125, 1784
- Johnston, H. M., Fender, R., & Wu, K. 1999, MNRAS, 308, 415
- Kallman, T., & Bautista, M. 2001, ApJS, 133, 221
- Kazanas, D., Hua, X.-M. & Titarchuk, L. G. 1997, ApJ, 480, 735
- Kaspi, S. et al. 2001, ApJ, 554, 216
- Königl, A. & Kartje, J. F. 1994, ApJ, 434, 446 (KK94)
- Kopko, M., Turnshek, D. A., & Espey, B. R. 1994, in IAU Symp. 159, Multiwavelength Continuum Emission of AGN, ed. T. Courvoisier & A. Blecha (Dordrecht:Kluwer), 450
- Krolik, J. H., McKee, C. F & Tarter, C. B. 1981, ApJ, 249, 422
- Mathur, S., Wilkes, B., Elvis, M., & Fiore, F. 1994, ApJ, 434, 493
- Mathur, S., Elvis, M., & Wilkes, B. 1995, ApJ, 452, 230
- McKernan, et al. 2007, MNRAS, 379, 1359
- Miller, J. M. et al, 2006, Nature, 441, 953
- Miller, J. M. 2007, ARA&A, 45, 411

- Miller, J. M., Raymond, J., Reynolds, C. S., Fabian, A. C., Kallman, T. R., & Homan, J. 2008, *ApJ*, 680, 1359
- Murray, N. et al. 1995, *ApJ*, 451, 498
- Narayan, R. & Yi, 1994, *ApJ*, 428, L13
- Neilsen, J., Remillard, R. A & Lee, J. C. 2012, *MNRAS*, 421, 502
- Netzer, H. et al. 2007, *ApJ*, 666, 806
- Nenkova, M. et al. 2008, *ApJ*, 685, 160
- Osterbrok, D. E. 1989, “Astrophysics of Gaseous Nebulae and Active Galactic Nuclei”, University Science Books (p. 330)
- Papadakis, I. E., Nandra, K. & Kazanas, D. 2001, *ApJ*, 554, L133
- Pounds, K. A., King, A. R., Page, K. L., & O’Brien, P. T. 2003, *MNRAS*, 346, 1025
- Pounds, K. A., & Page, K. L. 2006, *MNRAS*, 372, 1275
- Proga, D., Stone, J. M., & Kallman, T. R. 2000, *ApJ*, 543, 686
- Proga, D. 2003, *ApJ*, 585, 406
- Proga, D., Kallman, T. R. 2004, *ApJ*, 616, 688
- Reeves, J. N., O’Brien, P. T., & Ward, M. J. 2003, *ApJ*, 593, L65
- Reynolds, C. S. 1997, *MNRAS*, 286, 513
- Richards, G. T. et al. 2006, *ApJS*, 166, 470
- Rowan-Robinson, M. 1995, *MNRAS*, 272, 737
- Rowan-Robinson, M., Valtchanov, I. & Nandra, K. 2009, *MNRAS*, 397, 1326
- Schulz, N. S. & Brandt, W. N. 2002, *ApJ*, 572, 971
- Shakura, N. I., & Sunyaev, R. A. 1973, *A&A*, 24, 337
- Sim, S. A. 2005, *MNRAS*, 356, 531
- Sim, S. A., Long, K. S., Miller, L., & Turner, T. J. 2008, *MNRAS*, 388, 611
- Sim, S. A., Miller, L., Long, K. S., Turner, T. J., & Reeves, J. N. 2010 (arXiv:1002.0544)

- Srianand, R. & Petitjean, P. 2000, *A&A*, 357, 414
- Steffen, A. T. et al. 2006, *AJ*, 131, 2826
- Tananbaum, H., et al. 1979, *ApJ*, 234, L9
- Tombesi, F. et al. 2010a, *A&A*, 521, 57
- Tombesi, F. et al. 2010b, *ApJ*, 719, 200
- Tueller, J. 2008, *ApJ*, 681, 113
- Urry, M. C. & Padovani, P. 1995, *PASP*, 107, 803
- Weymann, R. J., Morris, S. L., Foltz, C. B., & Hewett, P. C. 1991, *ApJ*, 373, 23
- Zheng, Z. Y., & Wang, J. X. 2008, *ApJ*, 688, 116